frontiers | Frontiers in Energy Research

TYPE Original Research
PUBLISHED 06 February 2023
DOI 10.3389/fenrg.2023.1124621

Check for updates

OPEN ACCESS

EDITED BY
Nicholas P. Stadie,
Montana State University, United States

REVIEWED BY
Anozie Ebigbo,
Helmut Schmidt University, Germany
Vikram Vishal,
Indian Institute of Technology Bombay, India

*CORRESPONDENCE
Na Liu,
Na.Liu@uib.no

SPECIALTY SECTION
This article was submitted to Hydrogen Storage and Production, a section of the journal Frontiers in Energy Research

RECEIVED 15 December 2022
ACCEPTED 25 January 2023
PUBLISHED 06 February 2023

CITATION
Liu N, Kovscek AR, Fernø MA and Dopffel N (2023), Pore-scale study of microbial hydrogen consumption and wettability alteration during underground hydrogen storage.
Front. Energy Res. 11:1124621.
doi: 10.3389/fenrg.2023.1124621

COPYRIGHT
© 2023 Liu, Kovscek, Fernø and Dopffel. This is an open-access article distributed under the terms of the Creative Commons Attribution License (CC BY). The use, distribution or reproduction in other forums is permitted, provided the original author(s) and the copyright owner(s) are credited and that the original publication in this journal is cited, in accordance with accepted academic practice. No use, distribution or reproduction is permitted which does not comply with these terms.

Pore-scale study of microbial hydrogen consumption and wettability alteration during underground hydrogen storage

Na Liu[1]*, Anthony R. Kovscek[2], Martin A. Fernø[1,3] and Nicole Dopffel[3]

[1]Department of Physics and Technology, University of Bergen, Bergen, Norway, [2]Department of Energy Science & Engineering, Stanford University, Stanford, CA, United States, [3]Energy & Technology, NORCE Norwegian Research Centre AS, Bergen, Norway

Hydrogen can be a renewable energy carrier and is suggested to store renewable energy and mitigate carbon dioxide emissions. Subsurface storage of hydrogen in salt caverns, deep saline formations, and depleted oil/gas reservoirs would help to overcome imbalances between supply and demand of renewable energy. Hydrogen, however, is one of the most important electron donors for many subsurface microbial processes, including methanogenesis, sulfate reduction, and acetogenesis. These processes cause hydrogen loss and changes of reservoir properties during geological hydrogen storage operations. Here, we report the results of a typical halophilic sulfate-reducing bacterium growing in a microfluidic pore network saturated with hydrogen gas at 35 bar and 37°C. Test duration is 9 days. We observed a significant loss of H_2 from microbial consumption after 2 days following injection into a microfluidic device. The consumption rate decreased over time as the microbial activity declined in the pore network. The consumption rate is influenced profoundly by the surface area of H_2 bubbles and microbial activity. Microbial growth in the silicon pore network was observed to change the surface wettability from a water-wet to a neutral-wet state. Due to the coupling effect of H_2 consumption by microbes and wettability alteration, the number of disconnected H_2 bubbles in the pore network increased sharply over time. These results may have significant implications for hydrogen recovery and gas injectivity. First, pore-scale experimental results reveal the impacts of subsurface microbial growth on H_2 in storage, which are useful to estimate rapidly the risk of microbial growth during subsurface H_2 storage. Second, microvisual experiments provide critical observations of bubble-liquid interfacial area and reaction rate that are essential to the modeling that is needed to make long-term predictions. Third, results help us to improve the selection criteria for future storage sites.

KEYWORDS

hydrogen subsurface storage, microbial effects, microfluidic pore network, hydrogen consumption, contact angle, wettability

1 Introduction

Underground hydrogen storage (UHS) has been proposed as a reliable and safe technology to store large quantities of hydrogen (H_2), which is produced from a surplus of renewable electrical energy (power-to-gas). This stored H_2 can subsequently compensate the seasonal fluctuations in the supply and demand of renewable energy (Carden and Paterson, 1979; Muhammed et al., 2022). Current subsurface storage projects in Europe often concentrated on

storing H_2 in artificially constructed salt caverns, e.g., the HyUnder project (Landinger et al., 2014) because salt cavern storage is suggested to be suitable to short-to medium-term energy demand fluctuations (Heinemann et al., 2021a).

For long-term and large-scale H_2 storages, depleted oil and gas fields and saline aquifers are potential storage formations (Heinemann et al., 2018; Hemme and Van Berk, 2018), due to the large storage capability and well-known geological structure from former exploration (Zivar et al., 2021; Jafari Raad et al., 2022; Muhammed et al., 2022). The elevation of H_2 concentration following injection, however, may stimulate the growth of hydrogenotrophic microorganisms in the subsurface. This can have adverse implications for gas storage and withdrawal efficiency including microbial H_2 consumption, gas composition changes, clogging and corrosion (Dopffel et al., 2021; Thaysen et al., 2021). Several recent reviews discussed the potential microbial risks in subsurface H_2 storage and highlighted the importance of monitoring and controls of microbial activity in subsurface environments (Heinemann et al., 2021b; Dopffel et al., 2021; Zivar et al., 2021). Thaysen et al. (Thaysen et al., 2021) estimated the risk for microbial growth in 42 depleted oil and gas fields and showed that microbial growth and H_2 consumption will likely occur in low-salinity and low-temperature reservoirs.

Three microbial metabolisms are associated with the highest risks for implementing UHS: methanogenesis, sulfate reduction, and acetogenesis. The stored H_2 can be microbially converted to CH_4, H_2S, and CH_3COOH respectively. The activity of different microbial processes depends on the availability of microorganisms and electron acceptors such as sulfate or carbon dioxide in the reservoir (Dopffel et al., 2021). Especially, sulfate-reducing bacteria are commonly found in hydrocarbon reservoirs, which prefer temperatures around 38°C and near-neutral pH conditions (Schwartz and Postgate, 1985), but can also be active at high salinity of 24% (Ollivier et al., 1991) and temperatures above 100°C (Jørgensen et al., 1992). Sulfate-reducing bacteria can use sulfate as an electron acceptor to oxidize H_2 and generate H_2S, causing permanent H_2 loss and gas contamination (Ebigbo et al., 2013; Dopffel et al., 2021; Thaysen et al., 2021; Zivar et al., 2021). Due to their activity and growth, the high accumulation of bacterial cells can lead to the formation of biofilms and cause pore-clogging (microbial-induced clogging) near injection wells, resulting in dramatic decreases in gas injectivity (Eddaoui et al., 2021). A better understanding of microbial processes pertaining to subsurface H_2 storage is essential for precisely estimating the microbial risks and successful implementation at large-scale UHS in the future.

To date there is little experimental data on mechanisms of microbial H_2 consumption (Harris et al., 2007) and the effect of microbial growth on gas storage efficiency is not fully understood (Thaysen et al., 2021). In this work, we used a silicon-wafer micromodel with a pore pattern from natural sandstone for direct observations of the microbial-induced sulfate reduction at 35 bar and 37°C, representing the storage conditions of a shallow aquifer or a gas-water transition zone in a depleted gas field (Lysyy et al., 2022). A halophilic sulfate-reducing bacteria was cultured with H_2 gas for 9 days. Analysis of time-lapsed image series enabled quantitative studies of variation in pore-scale H_2 saturation, contact angle evolution and disconnection with microbial growth. Our results add new experimental data to explain the microbial processes during UHS, that are essential for modeling efforts which are needed to make long-term predictions and improve the selection criteria for future storage sites.

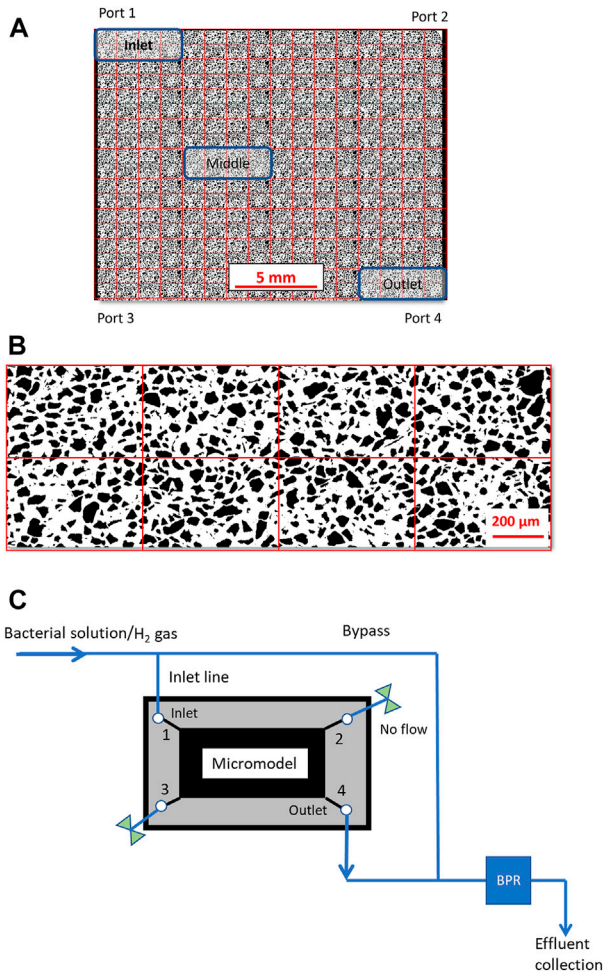

FIGURE 1
(A) The pore network (26.95 × 22.50 mm) was split into 16 columns and 18 rows for measurement of local biofilm/H_2 saturation and porosity. Units are shown as red boxes, and the blue rectangles represent the inlet, middle and outlet areas. **(B)** Binary image of the repeating unit of the porous network (1.65 × 1.14 mm) with black grains and white pore space. **(C)** Simplified schematic of the experimental setup to show the indented flow into the pore network. A more detailed description of the experimental setup can be found in our previous study (Benali et al., 2022).

2 Materials and methods

2.1 Bacterial strains and growth conditions

Desulfohalobium retbaense DSM 5692, a halophilic sulfate-reducing strain, was used as the model bacterium in this study. It can grow at pH ranging from 5.5–8.0, optimum temperature of 37°C and optimum salinity of 12% (Ollivier et al., 1991). Under anaerobic conditions, *Desulfohalobium retbaense* can utilize H_2 as an electron donor and sulfate as electron acceptor producing H_2S, for growth (Spring et al., 2010; Tinker et al., 2022). The organism was grown in the DSM 499 high salinity growth medium with some modifications: Base medium was: 1 g/L NH_4Cl, 0.3 g/L K_2HPO_4, 0.3 g/L KH_2PO_4, 20 g/L $MgCl_2{\cdot}6H_2O$, 100 g/L NaCl, 2.7 g/L $CaCl_2{\cdot}2H_2O$, 4 g/L KCl, 3 g/L Na_2SO_4, 1 mL/L trace element SL-10, 0.5 mL/L Na-resazurin solution (0.1% w/v), 0.3 g/L $Na_2S{\cdot}9\ H_2O$. 1.5 mL of a dense bacterial

solution was inoculated in 15 mL of base media amended with 80 mM sodium lactate, 40 mM sodium acetate, 0.3% yeast extract and 0.3% peptone solution at 37°C for 7 days under anaerobic conditions (N_2 headspace). This 7-day old culture was then used and injected into the micromodel.

2.2 Experimental setup and microfluidic pore network

The experimental setup consists of a high-pressure micromodel with a Zeiss microscope (Axio Zoom. V16, Zeiss) illuminating with a S ring cold-light (CL 9000 LED) source. This microscope setup was able to capture the whole pore network (total 121 separate images) with a resolution of 4.38 µm/pixel and acquisition time of 73 s. Pore space temperature was kept constant at 37°C ± 0.5°C by circulating warm water through internal copper tubes in the chip holder. Experimental pressure was controlled at 35 bar by a high precision plunger pump (Quizix Q5000-10 K), and a back pressure regulator (EB1ZF1 Equilibar Zero Flow) connected to a pressurized 300 mL N_2 cylinder. The experimental setup has a high-precision injection system with a constant dead-volume (10 µL before the pore network). The silicon micromodel capable of withstanding pressure up to 150 bar, was designed based on a thin section from a natural sandstone and the production procedures are found in (Buchgraber et al., 2012). The pore network constitutes of 36 repetitions of a unique pattern (Figure 1). The pore network has a porosity of 0.61 and pore volume of 11.1 µL. For image segmentation, the pore network was split into 288 units and units have a porosity range between 0.59 and 0.66. Three areas of interest (a unique pattern) have been identified at inlet, middle and outlet sites (blue rectangles in Figure 1A). The bottom silicon and top borosilicate glass have strongly hydrophilic surfaces due to the fabrication procedure where silicon is oxidized to SiO_2. Two open channels connect port 1 to 2 and port 3 to 4 across the injection and production sides of the micromodel. A more detailed description of the experimental setup and micromodel properties is found elsewhere (Benali et al., 2022).

2.3 Experimental procedure

The experimental procedure consists of the following steps:

1. Preparation: The pore space was flushed with ethanol, deionized (DI) water, and H_2O_2 (ACS reagent, 30 wt% solution in water, Thermo Scientific™) to clean all surfaces and waste from previous experiments, followed by > 100 pore volumes (PVs) of DI water.
2. Pressurization: The microfluidic system was pressurized to the operating pressure of 35 bar by flowing the growth medium at 50 µL/min from port 1 to port 4. The pressure was controlled by the back pressure regulator at the outlet.
3. Bacterial inoculation: To remove residual water in the pore network, approximately 40 PVs of growth medium were injected at 20 µL/min into the pore network. Then, 10 PVs of precultured bacterial solution were injected at 6 µL/min for inoculation and bacterial attachment to the pore space surfaces, followed by an 18 h of shut-in period. The period of bacterial inoculation was approximately 19 h.
4. H_2 drainage: H_2 was injected at 5 µL/min in the pore space for 4 h. The volumetric flowrate corresponds to a Darcy velocity of 10.15 mm/min. After gas breakthrough, 100 PVs of H_2 were continually injected into the pore network at the same injection rate.
5. Bacterial experiment: After drainage (i.e., 100 PVs of H_2 injected), all the tubing connected to the pore network were flushed with growth medium to remove H_2 and the microfluidic system was closed and incubated at 37°C for 7–9 days by flowing DI water through bypasses to maintain the system pressure. The spatiotemporal distribution of H_2 gas in the pore network was visualized by the high-resolution microscope system. The bacterial experiment started immediately after H_2 drainage (step 4. above), with a duration of 7–9 days.

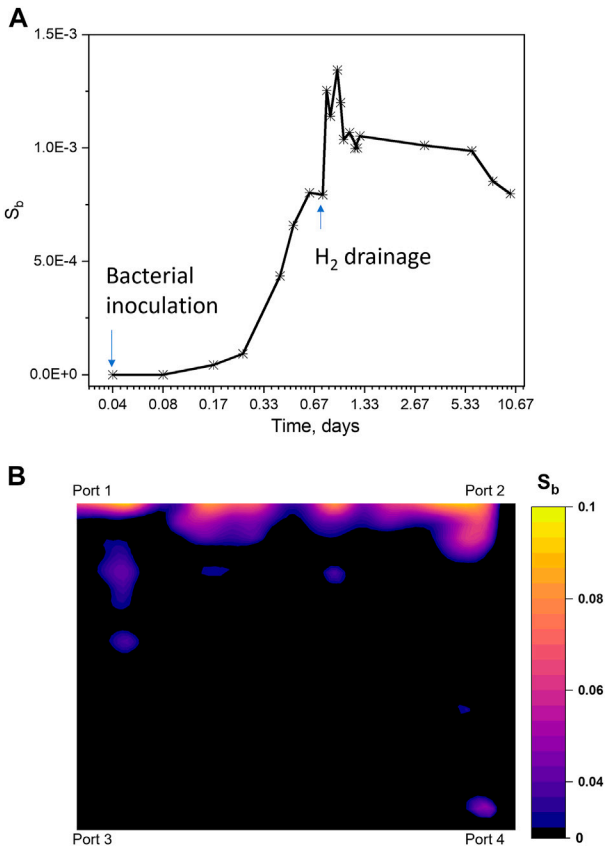

FIGURE 2
(A) Pore space biofilm growth during bacterial inoculation, H_2 drainage and microbial growth with H_2 processes in the pore network over time at 37°C and 35 bar. The biofilm saturation (S_b) was measured from high-resolution images of biofilms in the pore network over time (Supplementary Figure S1), with measurement uncertainty less than 1%. S_b equals the number of pixels of biofilms in the unit dividing with the number of pixels of pore space. Biofilms in the pore network were mainly formed during the bacterial inoculation stage and the saturation of biofilm in the pore network (S_b) was only $8{\cdot}10^{-4}$. During the bacterial inoculation process, some biofilms grew in the inlet line to port 1 (see Figure 1C). The flow of H_2 gas brought biofilms in the inlet line into the pore network, resulting in an increase of S_b (up to $1.3{\cdot}10^{-4}$). In the meantime, the shear stress from gas flow also caused the detachment of biofilms in the pore network. When microbial growth in H_2 gas, cells dispersed from biofilms caused a reduction of S_b. Note that the plot starts from bacterial inoculation and ends at bacterial growth with H_2 for 9 days. The horizontal axis uses a logarithmic scale. **(B)** Distribution of biofilms in the pore network after H_2 drainage (Day 1). Biofilms were mainly formed in the inlet regions (near port 1 and port 2) and partly blocked the pore throats near injection.

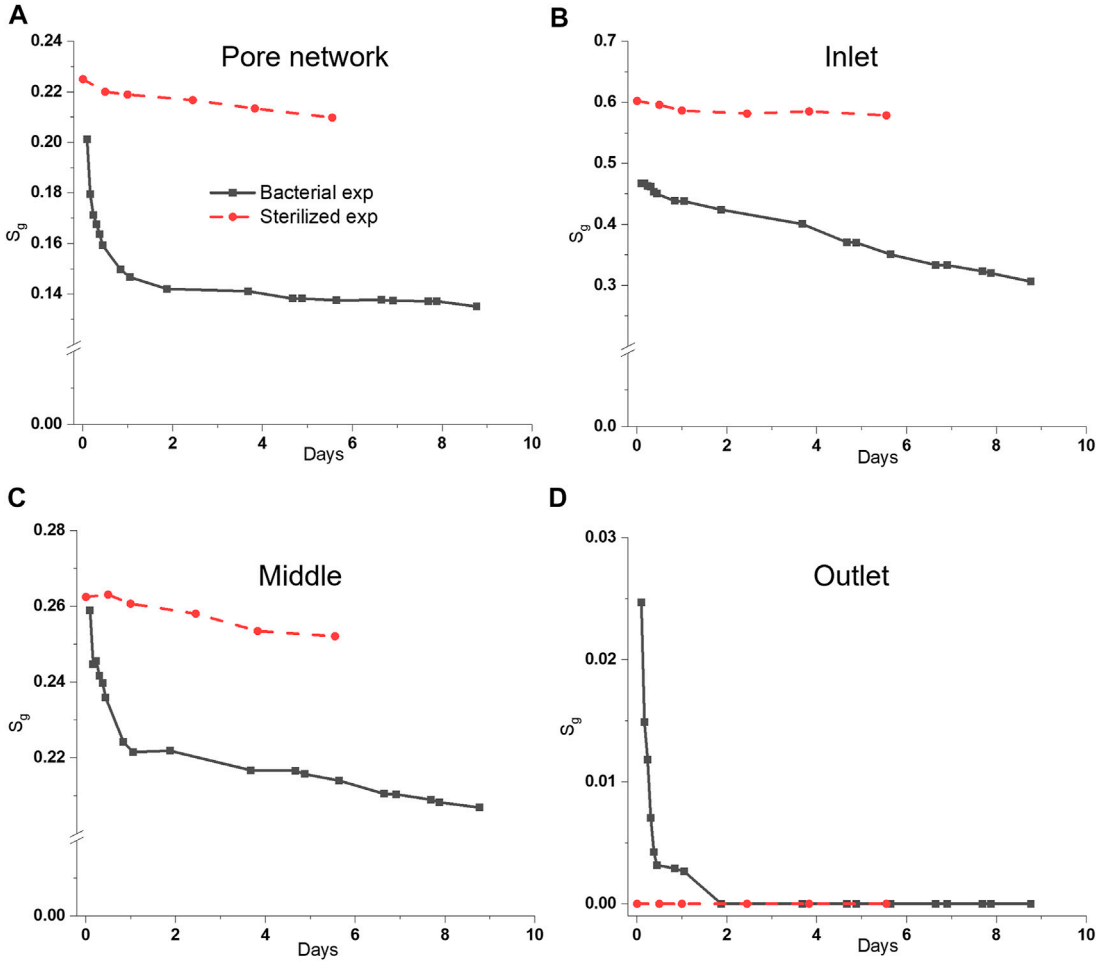

FIGURE 3
Plots of the dynamics of H_2 saturation in the whole pore network, inlet, middle and outlet areas during bacterial (black solid lines) and sterilized (red dash lines) experiments. Note that all plots start from the end of H_2 drainage, indicating that there is no loss from dissolution here. H_2 saturation (S_g) was quantified from the segmented 2D images with the maximum uncertainty of 12% (i.e., maximum error = 0.12 × S_g). Comparing the sterilized and bacterial experiment for the whole pore network **(A)**, the effect of bacterial consumption can be observed with more rapid decrease and lower S_g for the bacterial relative to the sterilized experiment. The gas saturation in the inlet **(B)** has a linear decrease during bacterial experiment, and a 34.5% reduction in S_g from microbial consumption (compared with 3.9% for sterilized conditions). The middle area **(C)** has the similar trend with the pore network that microbial cells consumed approximately 14% of H_2 in the first 2 days and only 6.9% in the next 7 days. Due to the low gas saturation in the outlet **(D)** from gas drainage, the gas phase was fully consumed in 2 days. Without microbial cells, the H_2 loss in the inlet and middle areas was 3.9% for 5 days and no H_2 gas was trapped in the outlet area.

A baseline, sterile experiment (i.e., without microbial cells) was performed with the experimental protocol detailed above. Each experiment was repeated twice with comparable results, and we discuss the main results using a single microbial experiment in Section 3 below. The repeated experiment demonstrates the same governing mechanisms for wettability change, microbial-induced H_2 loss and disconnection, although with higher initial H_2 saturation and lower biofilm saturation. The reader is referred to the Supplementary Material for more detail.

3 Results and discussion

3.1 Microbial-induced clogging

Microbial growth in porous media very often leads to biofilm formation and microbial-induced pore-clogging (Liu et al., 2019), and this was observed during bacterial inoculation and H_2 drainage processes in this work. Biofilms formed predominantly in the inlet area in less than 0.1% of the pore space after 18 h of growth. This is an expected result because *D. retbaense* is not a strong biofilm forming bacterium. We observed that some biofilms, however, blocked the flow of H_2 gas (Supplementary Figure S1) and reduced gas injectivity occurred. For instance, during H_2 drainage, the shear stress from gas flow pushed some biofilms formed in the injection line into the inlet area, and some biofilms detached from the pore network. There was, however, no new biofilm formation during microbial growth with H_2 gas and the biofilm saturation (S_b) reduced by 24% compared to S_b after drainage and culturing in H_2 for 9 days (Figure 2). Our hypothesis is that the biofilm reduction arises from a transition of bacterial lifestyle from biofilm-mode to planktonic-mode in a H_2-rich environment (Jefferson, 2004; Chua et al., 2014; Liu et al., 2019). This hypothesis is corroborated by earlier work (Liu et al., 2019) where biofilm detachment occurred in high nutrient environments, but

10.3389/fenrg.2023.1124621

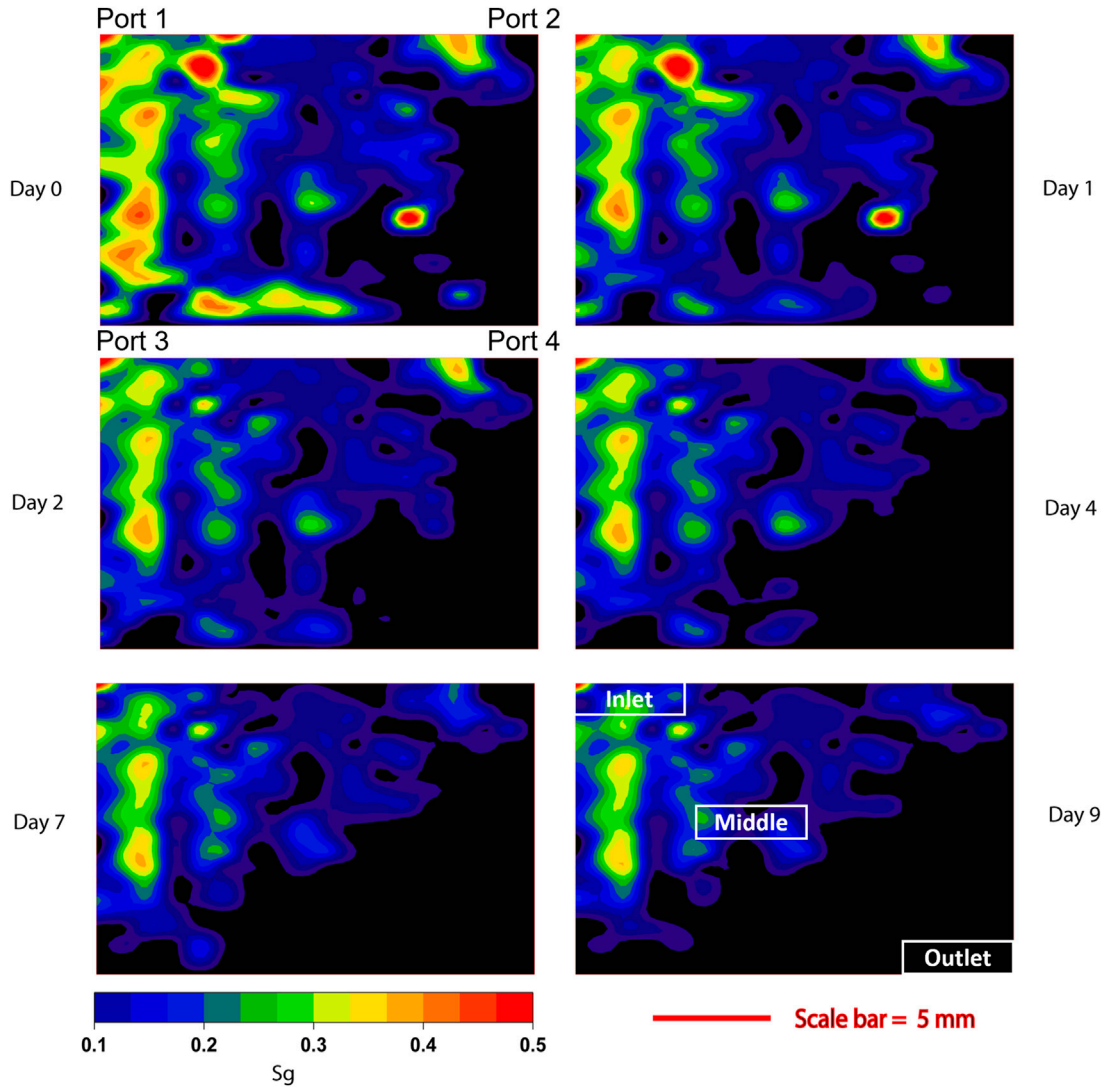

FIGURE 4
Contours plots of H_2 saturation (S_g) in the pore network during bacterial growth at 37 ± 0.5°C and 35 bar. The inlet area near port 1 initially (Day 0) had a higher gas saturation (0.61), while only a few H_2 bubbles saturated near port 4 ($S_g = 3.5{\cdot}10^{-3}$). After microbial growth with H_2 gas for 1 day, the gas saturation in the pore network was decreased from 0.201–0.146, where the average S_g reduction rate in each unit was 0.052 per day with a standard deviation of 0.0866. After Day 2, the reduction rate in each unit decreased to 0.009 per day and the H_2 bubbles in the outlet area were fully consumed by microbial cells. From Day 4, the consumption rate decreased to near zero revealing that the microbial activities were dramatically reduced after 4 days of culturing in H_2. To illustrate the S_g changes more clearly, contour lines in plots were smoothed with a parameter of $9.84{\cdot}10^{-4}$.

cannot be generalized for growth on H_2 based solely on the reported results: whether the lifestyle change is due to either reduced EPS formation or an active detachment process, and if whether cell numbers increased during this process, need to be investigated in future experiments. Our observations are only valid for the bacterial strain studied. Different microbial strains need to be investigated in the future to verify if this effect of H_2-induced biofilm detachment is common for many bacteria.

3.2 Microbial-induced H_2 loss

In this study, the main microbial process with UHS implications is hydrogenotrophic sulfate reduction (Ebigbo et al., 2013; Hemme and Van Berk, 2018; Gregory et al., 2019):

$$SO_4^{2-} + 4H_2 + H^+ \rightarrow HS^- + 4H_2O$$

The sulfate-reducing bacterium (*D. retbaense*) used H_2 (aq) as a source of electrons to reduce sulfate and generate H_2S. Figure 3 plots the changes of gas saturation in bacterial (solid lines) and sterilized (dash lines) experiments at inlet, middle and outlet areas (cf. Figure 1). Biofilm formation in the inlet area reduced gas injectivity (cf. Section 3.1) and initial H_2 saturation (S_{g0}) for the inlet area ($S_{g0} = 0.46$) compared with the sterilized experiment ($S_{g0} = 0.60$). Note that all plots start from the end of H_2 drainage. After 2 days of microbial growth with H_2 gas, the H_2 saturation (S_g) decreased by 29.4% due to the bacterial consumption, compared with 3.7% for the sterilized case (reduction in the sterilized case is believed to be a combined effect of system leakage and measurement uncertainty). In the following 4 days, the reduction of S_g in the bacterial experiment was low

($5{\cdot}10^{-3}$, and similar to the sterilized case), indicating less microbial activity. At the end of experiment (9 days), 32.9% of the initially stored H_2 gas was consumed by the microbial cells. The inlet area shows a constant bacterial consumption rate (reduction of S_g over time) of 0.018 per day (constant rate for entire experiment), which is lower compared to the middle (0.03) and outlet (0.025) area for the first 2 days. On average, the reduction in H_2 saturation was one order of magnitude larger for the bacterial case (0.024) relative to the sterilized case (0.0029). Similar results were obtained from the repeated experiment (Supplementary Figure S2A) that the consumption rate in the first 2 days is much faster than the following days. Note that the initial H_2 saturation for the inlet, middle and outlet was not the same, and the differences of consumption rate were related to the distribution of bacterial solution and H_2 gas in the pore network.

The spatial distribution of S_g per unit during bacterial consumption (Figure 4) showed that the gas phase in the inlet area initially was connected, compared with predominantly disconnected H_2 bubbles in the outlet area due to the effects of snap off (Singh et al., 2017; Lysyy et al., 2022). The variation of disconnected H_2 bubbles in the pore network will be detailed in Section 3.4. The microbial consumption rate in the pore network was strongly influenced by the interfacial area between gas and brine. Smaller H_2 bubbles improved the H_2 availability for microbial consumption due to i) increased H_2 dissolution and ii) larger contact area between H_2 gas and the microbial cells. We postulate that H_2 availability is a driving mechanism for the observed consumption efficiency and rate in the pore space. Rapid bacterial consumption (within 7 h) was observed in the outlet area, occupied with disconnected H_2 bubbles with large contact area. The consumption rate is also determined by activity of the microbial cells, exemplified by a drop in consumption rate (constant S_g) observed in whole pore network and middle area beyond 2 days. We attribute the observed rate reduction to changes of the microbial growing environment. We assume that both sulfate (electron acceptor) and acetate (carbon source) were still available at high concentration in the solution. The loss in activity might therefore be a result of other unfavorable conditions. Bacterial growth in a confined system will lead to formation of bioproducts and sometimes toxins accumulated in the aqueous phase. For example, increased H_2S/HS^- concentrations from sulfate reduction can be toxic to cells, even to sulfate-reducing cells. This, together with a noticeable pH increase during sulfate reduction, will be unfavorable for continued bacterial growth (Liu et al., 2019). We were unable to measure H_2S in the effluent due to the small volumes associated with microfluidic experiments. Hence, the mechanisms for the reduced activity need to be investigated further. Cells in the inlet area were less affected, most likely due to the presence of biofilms that are known to protect embedded cells from environmental stresses like pH change and toxins in the environment (Flemming and Wingender, 2010).

Due to the low solubility of H_2 in brine, H_2 loss from diffusion and dissolution will be small compared to microbial-induced loss (see the Supplementary Material) in agreement with previous numerical estimations (Carden and Paterson, 1979; Anikeev et al., 2021). Microbial consumption, however, is a major risk for H_2 storage at industrial scale, and specifically for the microbial sulfate reduction in our work. As sulfate compounds are common in subsurface reservoirs, deriving from the aqueous dissolution of mineral phases like anhydrite ($CaSO_4$) (Hemme and Van Berk, 2018), H_2 injection can trigger hydrogenotrophic sulfate reduction due to accelerated activity of sulfate-reducing microorganisms. H_2 can be microbially converted to H_2S (aq), resulting in H_2 loss (up to 32.9% in this study) and reservoir souring. Our results show that H_2 consumption rates vary over time due to changes in active microbial cells and mass transfer at the interface. Therefore, microbial induced H_2 loss pertaining to underground storage is determined by the reservoir conditions (T, p, pH), microbial cells (activity and density) and mass transfer at the interface. Previous theoretical studies have shown that consumption can vary from 0%–17% of the injected H_2, depending on the aquifer conditions and the involved microbial mechanisms (Thaysen et al., 2021). We measured H_2 consumption rates at high initial nutrient content, high initial cell numbers and optimal physicochemical conditions for the studied strain, hence, investigating a worst-case scenario for microbial H_2 loss for the oligotrophic subsurface. On the other hand, in the subsurface some effects will favor microbial consumption, for example buffering minerals (carbonates) which will stabilize pH leading to a prolonged microbial activity. Also, under certain flow conditions in the subsurface fresh nutrients and cells might be introduced into the storage area, resulting in a faster consumption rate in the late stage of gas storage compared to our confined system.

3.3 Microbial-induced wettability alteration

The drainage of H_2 into the pore network containing two solutions with the same salinity resulted in non-identical gas distribution (Figure 4; Supplementary Figure S3) as a result of microbial induced wettability alteration. The wettability changes were investigated by measuring the contact angle in a three-phase (gas-aqueous-grains) system, which was quantified with image analysis using open-source ImageJ software. The gas-liquid interfacial area reduced to near minimal values when the H_2 gas was exposed to the bacterial solution for 1 day (see images in Figure 5, Supplementary Figure S2B). Results indicate that the bacterial cells altered the surface wettability from an initial water-wet (41° contact angle) to a neutral-wet (average 96° contact angle), compared with an unchanged contact angle (28°) for the sterilized experiment. We assume that bioproduct and bacterial adhesion to the solid surfaces are the dominant mechanisms for the contact angle shift to increased hydrophobicity. Microbial cells growing within the water film around the H_2 gas phase can easily attach to the SiO_2 surface of the micromodel. The cell surface of microbes has wetting properties more neutral wet than the SiO_2 surface; thus, the wettability is altered depending on the nature of the bacterial cell's membrane structure. Similarly, the increased pH due to microbial growth can also result in increased hydrophobicity, that can be explained by the protonation state of the polar molecules and, thus the number of charged surface species at the interface of H_2/aqueous/SiO_2 (Santha et al., 2019).

Wettability is one of the key parameters that determines the storage capacity and gas recovery (Bai and Tahmasebi, 2022; Pan et al., 2022) for underground gas storage. With the increase of contact angles induced by microbes, the capillary entry pressure decreases resulting in more favorable drainage displacement efficiency. The contact angle near 90° also lead to minimal interfacial surface area and favorable gas recovery due to reduction in capillary pressure (Lin et al., 2019; Lin et al., 2021). This in turn leads to decreased, snapped-off, and disconnected gas phase and an increase in H_2 relative permeability during imbibition. Hence, a large percentage of gas can potentially be recovered from porous reservoir rock when all

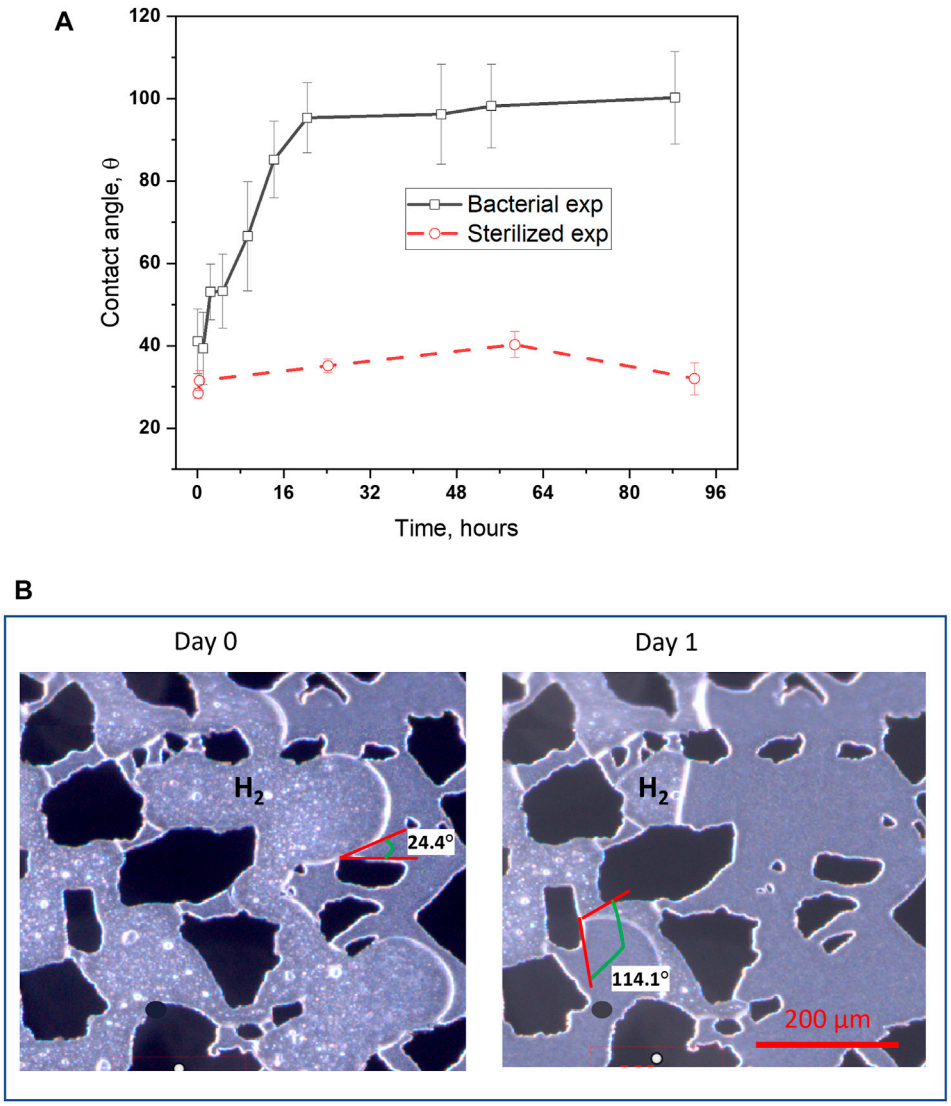

FIGURE 5
(A) The average contact angle in the bacterial experiment increased from 41°–96° within 20 h, while there was little variation in the sterilized experiment (kept at a constant of 33°). After 4 days, microbial cells changed the wettability of the SiO_2 surface to a neutral-wet state with the average contact angle of 100° and standard deviation of 11°. **(B)** Images of the increase of contact angle from Day 0–Day 1. The contact angle (θ) among H_2 gas, bacterial solution and solid grains ranges from 24.4°–114.1°.

other factors are equal. Accordingly, microbial growth induced minimal surface areas in the hydrogen-brine-SiO_2 system may enhance the gas storage efficiency of UHS operations.

3.4 Microbial-induced bubble disconnection

During H_2 drainage, gas-phase continuity can be broken by snap-off, generating isolated gas bubbles and trapping gas in the pore space (Lysyy et al., 2022). Due to the low H_2 drainage rate (the capillary number is $2.04{\cdot}10^{-8}$ and Pelect number equals 4.76) in our study, the initial saturation of isolated gas bubbles in the pore network was less than 0.01 after H_2 injection and mainly located in the outlet area (Figure 3). As discussed above, the microbial effects of bacterial consumption and the increase of contact angle can reallocate the residual H_2 phase in the pore network (see Figure 6). Initially, H_2 preferentially occupied the large, connected pore clusters with large pore throats. After bacterial consumption for 1 day, most of the residual H_2 remained in the same pores (red) but some movements into the neighboring pores were also observed (yellow). As the capillary entry pressure was reduced with the increase of contact angle, more and more H_2 bubbles were able to enter the nearby pores with smaller pore throats. The disconnection of gas phase (S_{gi}) in the pore network was measured by dividing the number of pixels of disconnected bubbles with the number of pixels of pore space. The plot in Figure 6A indicates that the disconnection of the H_2 phase in the pore network increased up to 72.8% for 5 h, while the sterilized experiment increased only 22.6% and stayed at a constant value until the end of experiment.

Bacterial consumption can break the continuity of the gas phase and generate isolated gas bubbles, which further increases the contact area of H_2 and microbial cells and then accelerated the gas

10.3389/fenrg.2023.1124621

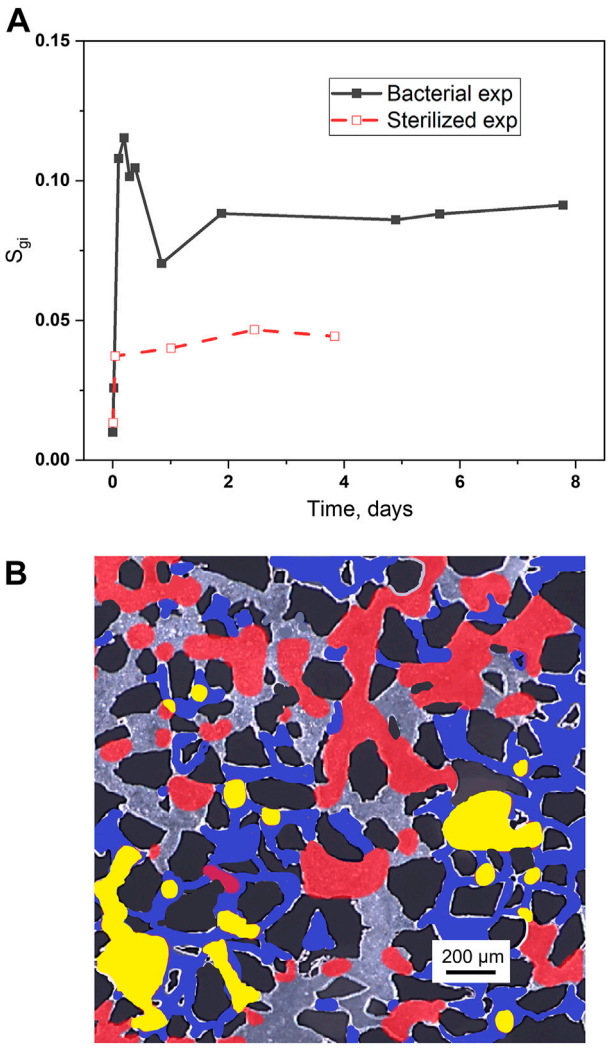

FIGURE 6
(A) Saturation of disconnected H_2 bubbles (S_{gi}) over time with bacterial (black, solid) and sterilized (red, dashed) aqueous solutions. **(B)** Dynamics of H_2 bubbles over 24 h: initially the H_2 gas was distributed in large, connected pore clusters with large pore throats (grey + red), and the aqueous phase saturated the remaining pores (blue + yellow). The H_2 bubble distribution changed over 24 h (red + yellow), where red represents the H_2 bubbles that remained in the same pore clusters and yellow represents H_2 bubbles with new pore occupancy. The aqueous phase distribution after 24 h (blue + grey) increased relative to initial conditions. The black represents silicon grains in the micromodel, and remain stationary during the experiment. We assume that the redistribution of gas after 24 h is partly due to contact angle changes and increased hydrophobicity.

consumption rate. Therefore, a decrease of S_{gi} was observed after 7 h as a result of the fast consumption of isolated gas bubbles. The same trend was observed in the repeating experiment (see Supplementary Figure S2C). Our pore-scale results reveal that microbial consumption and wettability alteration are the two main mechanisms that determine disconnection and entrapment of the gas phase in the pore network. The increase of disconnection of H_2 gas will reduce gas mobility dramatically in the receiving reservoir (Alhosani et al., 2021). Furthermore, the blockage of gas bubbles at the entrance will increase the flow resistance (Jian et al., 2022), causing a low gas recovery. Most of the trapped H_2 bubbles in the high permeability zones will be immobile in the subsequent injection cycles, hence, are difficult to recover.

The microbial effects on disconnection of H_2 gas can be summarized as the following: the increase of contact angles induced by microbes can reduce the capillary entry pressure and decrease the snapped-off and disconnected gas phase during imbibition; the stored H_2 phase, however, can be consumed by microbial cells forming new disconnected H_2 bubbles in the pore.

3.5 Implications for H_2 underground storage in porous systems

The aim of UHS is to store large amounts of H_2 gas from surplus production of renewable electricity to mitigate seasonal fluctuations in energy supply and demand (Amid et al., 2016; Heinemann et al., 2021b; Dopffel et al., 2021). Because H_2 is an import electron donor for microorganisms, assessment of microbial effects for UHS is an inevitable step to estimate the potential risks for gas injectivity, H_2 loss and recovery for large-scale H_2 geo-storage operations (Anikeev et al., 2021). In our study, we investigated one of the major H_2 consuming processes in the subsurface, bacterial sulfate reduction under high salinity conditions. Overall, four microbial effects were observed in our experiments: microbial induced-clogging, H_2 loss from bacterial consumption, wettability alteration, and increased residual trapping of the H_2 phase.

Microbial-induced wettability alteration appears to be a positive effect of microbial growth in a H_2 storage reservoir: increased hydrophobicity resulted in the presence of minimal gas-liquid surface areas, and high recovery efficiency, due to reduction in capillary pressure and high gas relative permeability. In contrast, the other observed microbial effects are expected to affect adversely the storage efficiency.

Biofilm formation in the near-well regions may reduce H_2 injectivity and change the subsurface transport properties. The risk of H_2 loss from dissolution and diffusion in the brine is limited due to low solubility, but permanent loss from microbial consumption must be considered for economic reasons, particular for storage in aquifers due to the abundance of sulfate-reducing microorganisms and sulfate in the formation water (Zivar et al., 2021). The production of hazardous gases, such as H_2S would lead to contamination of the injected H_2. The increase of disconnected H_2 bubbles in the pore network will also speed up the microbial consumption process due to increased interfacial area and increase the flow resistance, resulting in a low gas recovery.

Whether all these microbial effects will be at play during H_2 storage will depend on field specific factors like the indigenous microbial community, cell numbers, available nutrients and sulfate. In two major H_2 storage field trials (Underground Sun Project, Austria, and HyChico, Argentina) microbial activity was reported as an important factor for H_2 loss, but without indications of active sulfate-reducing microbes because both reservoirs were low in sulfate and the major microbial activity was methanogenesis ($H_2 + CO_2 = CH_4$) (Bauer and Austria, 2017). However, a recent study showed significant microbial hydrogen consumption with sulphate reduction in original brine from a gas reservoir (Dohrmann and Krüger, 2023). The overall risk will depend on the field specific microbial communities and field characteristics. That means that further field trials need to show if the mechanisms described in our work will be observed in the field. Our results help in understanding and interpreting field test data and to avoid significant H_2 losses.

4 Conclusion

Our pore-scale analysis provided a comprehensive characterization of microbial effects of a typical halophilic sulfate-reducing bacterium during geological H_2 storage operations within a porous network. We showed that the microbial activity during H_2 storage may have important implications for H_2 recovery, gas injectivity and reservoir properties. Considering the small scale and small volumes of our micromodels and the optimal culturing conditions, the estimation of H_2 loss rates from microbial consumption cannot directly be linked to large-scale operations to quantify the extent of the effects in a reservoir. Core-scale experiments and simulations are needed to further estimate the net positive or negative effect of microbial growth. As UHS has received a lot of attention as a technically feasible technology to store renewable energy and thereby mitigate climate change, the microbial risks need to be explored in more detail to avoid storage failure or even storage souring by H_2S. Future laboratory research should not only focus on single strains but also use original field communities from potential storage locations. Furthermore, the influence of H_2 on microbial living styles and also on rock properties in the underground storage site must be investigated further.

Data availability statement

The original contributions presented in the study are included in the article/Supplementary Material, further inquiries can be directed to the corresponding author.

Author contributions

NL: Conceptualization, Methodology, Writing. AK: Methodology, Writing—review & editing. MF: Supervision, Funding acquisition, Writing—review and editing. ND: Conceptualization, Writing.

Funding

We acknowledge financial support from by the Research Council of Norway under the following projects: Hydrogen Storage in Subsurface Porous Media-Enabling Transition to Net-Zero Society (project No. 325457), and Centre for Sustainable Subsurface Resources (project No. 331841).

Acknowledgments

The authors would like to thank Benyamine Benali, Oscar E. Medina and Jhon Fredy Gallego Arias for the assistant in image processing.

Conflict of interest

The authors declare that the research was conducted in the absence of any commercial or financial relationships that could be construed as a potential conflict of interest.

Publisher's note

All claims expressed in this article are solely those of the authors and do not necessarily represent those of their affiliated organizations, or those of the publisher, the editors and the reviewers. Any product that may be evaluated in this article, or claim that may be made by its manufacturer, is not guaranteed or endorsed by the publisher.

Supplementary material

The Supplementary Material for this article can be found online at: https://www.frontiersin.org/articles/10.3389/fenrg.2023.1124621/full#supplementary-material

References

Alhosani, A., Selem, A. M., Lin, Q., Bijeljic, B., and Blunt, M. J. (2021). Disconnected gas transport in steady-state three-phase flow. *Water Resour. Res.* 57 (12), e2021WR031147. doi:10.1029/2021WR031147

Amid, A., Mignard, D., and Wilkinson, M. (2016). Seasonal storage of hydrogen in a depleted natural gas reservoir. *Int. J. hydrogen energy* 41 (12), 5549–5558. doi:10.1016/j.ijhydene.2016.02.036

Anikeev, D. P., Zakirov, E. S., Indrupskiy, I. M., and Anikeeva, E. S. (2021). "Estimation of diffusion losses of hydrogen during the creation of its effective storage in an aquifer," in Paper presented at the SPE Russian Petroleum Technology Conference, Virtual, October, 2021. doi:10.2118/206614-MS

Bai, T., and Tahmasebi, P. (2022). Coupled hydro-mechanical analysis of seasonal underground hydrogen storage in a saline aquifer. *J. Energy Storage* 50, 104308. doi:10.1016/j.est.2022.104308

Bauer, S., and Austria, R. (2017). *Underground Sun storage*. Austria: Final Report Vienna, 1369.

Benali, B., Foyen, T. L., Alcorn, Z. P., Haugen, M., Gauteplass, J., Kovscek, A. R., et al. (2022). Pore-scale bubble population dynamics of CO2-foam at reservoir pressure. *Int. J. Greenh. Gas Control* 114, 103607. doi:10.1016/j.ijggc.2022.103607

Buchgraber, M., Al-Dossary, M., Ross, C. M., and Kovscek, A. R. (2012). Creation of a dual-porosity micromodel for pore-level visualization of multiphase flow. *J. Petroleum Sci. Eng.* 86-87, 27–38. doi:10.1016/j.petrol.2012.03.012

Carden, P., and Paterson, L. (1979). Physical, chemical and energy aspects of underground hydrogen storage. *Int. J. Hydrogen Energy* 4 (6), 559–569. doi:10.1016/0360-3199(79)90083-1

Chua, S. L., Liu, Y., Yam, J. K. H., Chen, Y., Vejborg, R. M., Tan, B. G. C., et al. (2014). Dispersed cells represent a distinct stage in the transition from bacterial biofilm to planktonic lifestyles. *Nat. Commun.* 5 (1), 4462–4512. doi:10.1038/ncomms5462

Dohrmann, A. B., and Krüger, M. (2023). Microbial H2 consumption by a formation fluid from a natural gas field at high-pressure conditions relevant for underground H2 storage. *Environ. Sci. Technol.* 57 (2), 1092–1102. doi:10.1021/acs.est.2c07303

Dopffel, N., Jansen, S., and Gerritse, J. (2021). Microbial side effects of underground hydrogen storage - knowledge gaps, risks and opportunities for successful implementation. *Int. J. Hydrogen Energy* 46 (12), 8594–8606. doi:10.1016/j.ijhydene.2020.12.058

Ebigbo, A., Golfier, F., and Quintard, M. (2013). A coupled, pore-scale model for methanogenic microbial activity in underground hydrogen storage. *Adv. water Resour.* 61, 74–85. doi:10.1016/j.advwatres.2013.09.004

Eddaoui, N., Panfilov, M., Ganzer, L., and Hagemann, B. (2021). Impact of pore clogging by bacteria on underground hydrogen storage. *Transp. Porous Media* 139 (1), 89–108. doi:10.1007/s11242-021-01647-6

Flemming, H. C., and Wingender, J. (2010). The biofilm matrix. *Nat. Rev. Microbiol.* 8 (9), 623–633. doi:10.1038/nrmicro2415

Gregory, S. P., Barnett, M. J., Field, L. P., and Milodowski, A. E. (2019). Subsurface microbial hydrogen cycling: Natural occurrence and implications for industry. *Microorganisms* 7 (2), 53. doi:10.3390/microorganisms7020053

Harris, S. H., Smith, R. L., and Suflita, J. M. (2007). *In situ* hydrogen consumption kinetics as an indicator of subsurface microbial activity. *FEMS Microbiol. Ecol.* 60 (2), 220–228. doi:10.1111/j.1574-6941.2007.00286.x

Heinemann, N., Alcalde, J., Miocic, J. M., Hangx, S. J., Kallmeyer, J., Ostertag-Henning, C., et al. (2021). Enabling large-scale hydrogen storage in porous media–the scientific challenges. *Energy & Environ. Sci.* 14 (2), 853–864. doi:10.1039/d0ee03536j

Heinemann, N., Alcalde, J., Miocic, J. M., Hangx, S. J. T., Kallmeyer, J., Ostertag-Henning, C., et al. (2021). Enabling large-scale hydrogen storage in porous media – The scientific challenges. *Energy & Environ. Sci.* 14 (2), 853–864. doi:10.1039/D0EE03536J

Heinemann, N., Booth, M., Haszeldine, R. S., Wilkinson, M., Scafidi, J., and Edlmann, K. (2018). Hydrogen storage in porous geological formations–onshore play opportunities in the midland valley (Scotland, UK). *Int. J. Hydrogen Energy* 43 (45), 20861–20874. doi:10.1016/j.ijhydene.2018.09.149

Hemme, C., and Van Berk, W. (2018). Hydrogeochemical modeling to identify potential risks of underground hydrogen storage in depleted gas fields. *Appl. Sci.* 8 (11), 2282. doi:10.3390/app8112282

Jafari Raad, S. M., Leonenko, Y., and Hassanzadeh, H. (2022). Hydrogen storage in saline aquifers: Opportunities and challenges. *Renew. Sustain. Energy Rev.* 168, 112846. doi:10.1016/j.rser.2022.112846

Jefferson, K. K. (2004). What drives bacteria to produce a biofilm? *FEMS Microbiol. Lett.* 236 (2), 163–173. doi:10.1111/j.1574-6968.2004.tb09643.x

Jian, T., Chen, Q., Zhong, C., Qin, Y., and Xi, Z. (2022). Pore-scale systematic study on the disconnection of bulk gas phase during water imbibition using visualized micromodels. *Phys. Fluids* 34 (6), 062015. doi:10.1063/5.0094930

Jørgensen, B. B., Isaksen, M. F., and Jannasch, H. W. (1992). Bacterial sulfate reduction above 100°C in deep-sea hydrothermal vent sediments. *Science* 258 (5089), 1756–1757. doi:10.1126/science.258.5089.1756

Landinger, H., Buenger, U., Raksha, T., Weindorf, W., Simon, J., Correas, L., et al. (2014). *HyUnder- Hydrogen underground storage at large scale: Update of benchmarking of large scale hydrogen underground storage with competing options deliverable*, 1–74.

Lin, Q., Bijeljic, B., Berg, S., Pini, R., Blunt, M. J., and Krevor, S. (2019). Minimal surfaces in porous media: Pore-scale imaging of multiphase flow in an altered-wettability Bentheimer sandstone. *Phys. Rev. E* 99 (6), 063105. doi:10.1103/PhysRevE.99.063105

Lin, Q., Bijeljic, B., Foroughi, S., Berg, S., and Blunt, M. J. (2021). Pore-scale imaging of displacement patterns in an altered-wettability carbonate. *Chem. Eng. Sci.* 235, 116464. doi:10.1016/j.ces.2021.116464

Liu, N., Skauge, T., Landa-Marbán, D., Hovland, B., Thorbjørnsen, B., Radu, F. A., et al. (2019). Microfluidic study of effects of flow velocity and nutrient concentration on biofilm accumulation and adhesive strength in the flowing and no-flowing microchannels. *J. Industrial Microbiol. Biotechnol.* 46 (6), 855–868. doi:10.1007/s10295-019-02161-x

Lysyy, M., Ersland, G., and Fernø, M. (2022). Pore-scale dynamics for underground porous media hydrogen storage. *Adv. Water Resour.* 163, 104167. doi:10.1016/j.advwatres.2022.104167

Muhammed, N. S., Haq, B., Al Shehri, D., Al-Ahmed, A., Rahman, M. M., and Zaman, E. (2022). A review on underground hydrogen storage: Insight into geological sites, influencing factors and future outlook. *Energy Rep.* 8, 461–499. doi:10.1016/j.egyr.2021.12.002

Ollivier, B., Hatchikian, C. E., Prensier, G., Guezennec, J., and Garcia, J. L. (1991). Desulfohalobium retbaense gen. Nov., sp. nov., a halophilic sulfate-reducing bacterium from sediments of a hypersaline lake in Senegal. *Int. J. Syst. Evol. Microbiol.* 41 (1), 74–81. doi:10.1099/00207713-41-1-74

Pan, B., Ni, T., Zhu, W., Yang, Y., Ju, Y., Zhang, L., et al. (2022). Mini review on wettability in the methane–liquid–rock system at reservoir conditions: Implications for gas recovery and geo-storage. *Energy & Fuels* 36 (8), 4268–4275. doi:10.1021/acs.energyfuels.2c00308

Santha, N., Cubillas, P., and Greenwell, C. (2019). The effect of salinity and pH on wettability alteration of kaolinite films studied by contact. *Angle Meas.* 2019 (1), 1–17. doi:10.3997/2214-4609.201900172

Schwartz, W., and Postgate, J. R. (1985). the sulfate-reducing bacteria (2nd edition) X + 208 S., 20 abb., 4 tab. University press, cambridge 1983. US $ 39.50. *J. Basic Microbiol.* 25 (3), 202. doi:10.1002/jobm.3620250311

Singh, K., Menke, H., Andrew, M., Lin, Q., Rau, C., Blunt, M. J., et al. (2017). Dynamics of snap-off and pore-filling events during two-phase fluid flow in permeable media. *Sci. Rep.* 7 (1), 5192. doi:10.1038/s41598-017-05204-4

Spring, S., Nolan, M., Lapidus, A., Rio, T., Copeland, A., Tice, H., et al. (2010). Complete genome sequence of Desulfohalobium retbaense type strain (HR100T). *Stand. genomic Sci.* 2, 38–48. doi:10.4056/sigs.581048

Thaysen, E. M., McMahon, S., Strobel, G. J., Butler, I. B., Ngwenya, B. T., Heinemann, N., et al. (2021). Estimating microbial growth and hydrogen consumption in hydrogen storage in porous media. *Renew. Sustain. Energy Rev.* 151, 111481. doi:10.1016/j.rser.2021.111481

Tinker, K., Lipus, D., Gardiner, J., Stuckman, M., and Gulliver, D. (2022). The microbial community and functional potential in the midland basin reveal a community dominated by both thiosulfate and sulfate-reducing microorganisms. *Microbiol. Spectr.* 10 (4), e0004922. doi:10.1128/spectrum.00049-22

Zivar, D., Kumar, S., and Foroozesh, J. (2021). Underground hydrogen storage: A comprehensive review. *Int. J. Hydrogen Energy* 46 (45), 23436–23462. doi:10.1016/j.ijhydene.2020.08.138